J Musculoskelet Neuronal Interact 2009; 9(2):99-108

Original Article

Hylonome

Prediction of local cellular deformation in bone – Influence of microstructure dimensions

C.A. Apostolopoulos and D.D. Deligianni

Department of Mechanical Engineering and Aeronautics, University of Patras, Rion 26500, Greece

Abstract

A multilevel finite element approach is applied to predict local cell deformations in bone tissue. The loads applied to a whole femur during the stance phase of the gait cycle were related to the strain at the level of a single lacuna and of canaliculi. Cell deformations were predicted from detailed linear FE analysis of the microstructure, consisting of an arrangement of cells embedded in bone matrix material. The local macroscopic stress assigned to each point was used to calculate the mesoscopic and consequently the microscopic nodal forces. The actual tissue principal strain along the femur deviated considerably from an average tissue value. The predicted bone matrix strains around osteocyte lacunae and canaliculi, were nonuniform and differed significantly from the macroscopically measured strains. Peak stresses and strains in the walls of the lacuna were up to six times those in the bulk extracellular matrix. Significant strain concentrations were observed at sites where the process meets the cell body. The dimensions of the lacunar axes influenced slightly the local strain.

Keywords: Finite Element Model, Microstructure, Cell Local Strain, Lacunar Axis

Introduction

Bone adapts to its mechanical environment and it has been presumed that this adaptation is stimulated by either strain or some strain-related quantity. Mechanical force applied to bone produces two localized mechanical signals on the cell: deformation of the extracellular matrix (substrate strain) and extracellular fluid flow-induced shear stresses and streaming potentials. Cowin et al. (1991)[1] proposed that osteocytes are mechanically activated by interstitial fluid flow through the lacunocanalicular porosity rather than by the bulk strains resulting from loading the whole bone. This proposal was strengthened by findings that *in vitro* strains of the order of 10,000 to 30,000 μstrain were required to obtain an increased cellular production of osteopontin mRNA and nitric oxide comparable to response to fluid flow[2,3].

It has been assumed that the maximum physiological levels of strain experienced by bones are those measured experimentally by strain gauges *in vivo* on the external bone surfaces up to 2,500 μstrain in humans. However, local strain can reach levels several times greater than the macroscopic fracture strain and possibly this stimulus is significant for bone adaptation. Experimentally it has been found that a nominal continuum strain level of 2,000 μstrain induces local, osteocyte level strains as high as 12,000 to 15,000 μstrain[4,5]. Trabecular tissue stress and strain estimates from global loading of whole bones have been found to be three[6] or three hundred times[7] that predicted by analyzing trabecular bone as a continuum.

In a work of this group[8] the loads applied to a whole femur during the stance phase of the gait cycle were related to the strain of a single lacuna and of canaliculi using a multilevel finite element model analysis. It was found that the micromorphology of osteocytarian canaliculi network produces an amplification of the strain observed at the continuum level sufficient to move the strain experienced by the osteocytes within the lacunae to a level above 10,000 microstrain, for which *in vitro* studies observe a direct mechanosensitivity of the osteocytes. The used simplified loading configuration (consisting of hip contact, abductors and ilio-tibial band) resulted in a significant overestimation of strain at the distal diaphyseal area[9].

The authors have no conflict of interest.

Corresponding author: D.D. Deligianni, Biomedical Engineering Lab, Department of Mechanical Engineering and Aeronautics, University of Patras, Rion 26500, Greece
E-mail: deligian@mech.upatras.gr

Accepted 19 January 2009

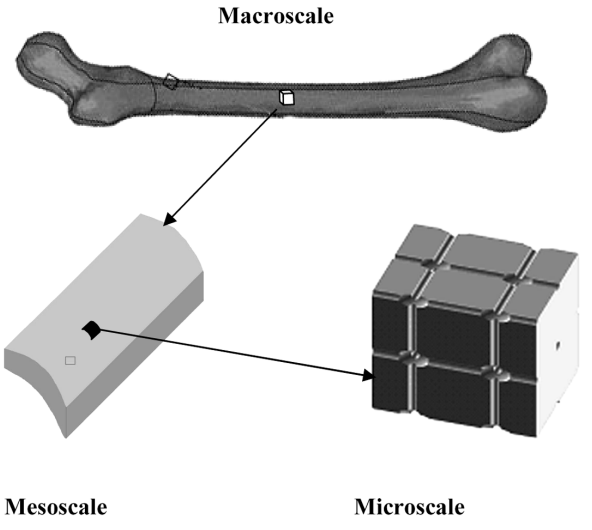

Figure 1. Multi-level analysis for the prediction of the strain field in the vicinity of an osteocyte. Macroscale level: a whole femur. Mesoscale level: a quadrant of the cylindrical shell of femur diaphysis. Microscale level: a periodic array of lacunae interconnected through canaliculi.

Previously, multilevel approaches have been successfully applied to describe heterogeneous technical materials[10]. Multi-scale finite element models were also developed to predict local cell deformations in the extracellular matrix of a cartilage explant[11] and in a skeletal muscle tissue construct[12].

In this work, a multilevel FE approach was applied to predict local stress and strain field at the cellular level in bone tissue using a loading configuration system of the femur which simulates optimally the *in vivo* loading conditions during walking. Strain was predicted from linear FE analysis of the microstructure, consisting of an arrangement of cells embedded in bone matrix material and the interconnecting canaliculi. The influence of the dimensions of the lacunar axes on the tissue strain in the cell microenvironment was examined.

Materials and methods

The microscopic length scale of a lacuna is orders of magnitude smaller than the macroscopic dimensions of a whole femur. In order to overcome the difficulties from the enormous difference in length scales involved, the analysis was divided into three separate problems. A FE analysis of the macroscale problem was performed to determine the strain

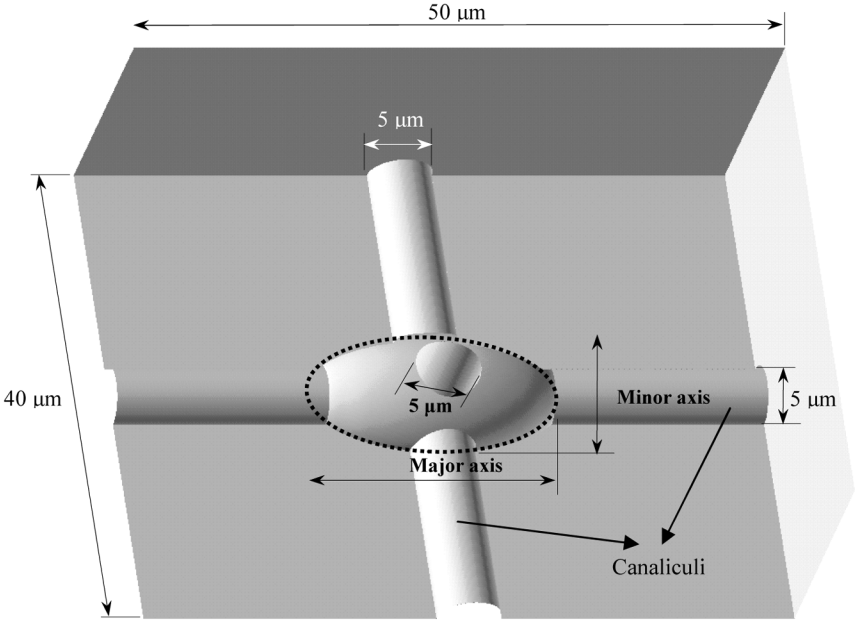

	Major axis	Minor axis
Geometry 1 (G1)	10 μm	5 μm
Geometry 2 (G2)	15 μm	7.5 μm
Geometry 3 (G3)	20 μm	10 μm

Figure 2. Geometry and dimensions of the model of the bone tissue surrounding a lacuna and the connected to it canaliculi.

distribution of the femur during one-legged stance. The results of the macroscale FE analysis were used to define the applied boundary conditions of a separate mesoscale FE model, representing a quadrant of the cylindrical shell of femur diaphysis with length of 10 mm. In turn, the results of the mesoscale FE analysis were used to determine boundary conditions for a microscale FE model, representing one osteocyte lacuna, surrounded by bone tissue, with the emerging canaliculi (Figure 1).

Cortical bone was assumed to be linearly elastic, homogeneous and transversely isotropic with a Young's modulus of 17 GPa and Poisson ratio of 0.41 in the axial direction and 11.5 GPa and 0.38 in the transverse directions, respectively[13,14]. The same material properties values were used in the macroscopic and mesoscopic levels of analysis. Cancellous bone was assumed to be isotropic material with E=206 MPa and Poisson ratio of 0.33[15]. The hypothesis of transversely isotropic material is very close to the real mechanical behavior of cortical bone material. The values of Young's modulus of cortical bone tissue in the transverse directions of the femoral shaft are nearly equal (less than 10% differences) and about 30% lower than those in the longitudinal direction[13,16].

The cortical and cancellous bone geometry was reconstructed three-dimensionally with data provided by the Internet site http://www.tecno.ior.it/VRLAB. The mesh of the femur geometry consisted of 5469 tetrahedral 10-noded SOLID 92 elements of ANSYS® (v. 8.1) FE code.

The used musculoskeletal system of the hip, developed by Heller et al. (2005), represented the simplest model of the hip muscles resulting in physiological-like hip joint loading throughout the entire gait cycles. The single instant of maximum *in vivo* hip contact force in the walking cycle was taken to define the load profile[17]. The hip contact force acts at P0 (Figure 3). The attachments or wrapping points of the muscles involved in walking are labelled P1 and P2. The values of muscle and joint reaction forces are displayed in Table 1.

The boundary condition, applied to the model of the femur, was full constraint of all degrees of freedom at the nodes (gray scale, Figure 4) that lie at the distal end of the femur (knee joint). The mesoscale FE model was discritized using the same element type as in the macroscale model (SOLID 92). A total of 10,432 elements were used. To couple the mesoscale FE analysis to the macroscale FE problem, the local macroscopic stress assigned to a certain macroscopic point (Figure 1) was used to calculate the mesoscopic nodal forces, which were used as external loads at the mesoscale analysis. A linear interpolation of these values was applied to the nodal points on the faces of the mesoscale model. These nodal forces are depicted in Figure 5 and their values are presented in Table 2.

The microstructural FE model has been described in a previous study[8]. Briefly, a three-dimensional model of a periodic array of lacunae and the interconnecting them canaliculi was formed as a part of the bone tissue. Lacunae shapes were assumed to be ellipsoid inclusions within the extracellular matrix, interconnected with cylindrical channels representing

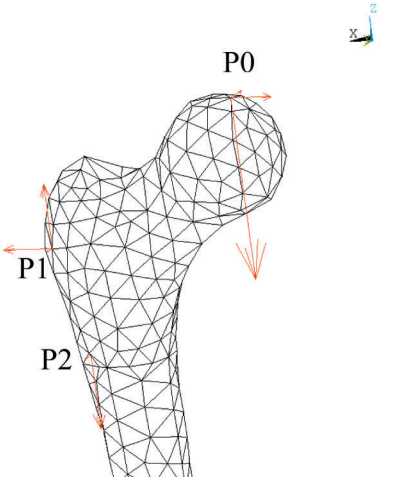

Figure 3. Loading configuration of the femur which resulted in physiological-like hip joint loading throughout the gait cycle (Heller et al., 2005). P0 is the point of application of the hip contact force. The wrapping points of the muscles are labelled P1 and P2.

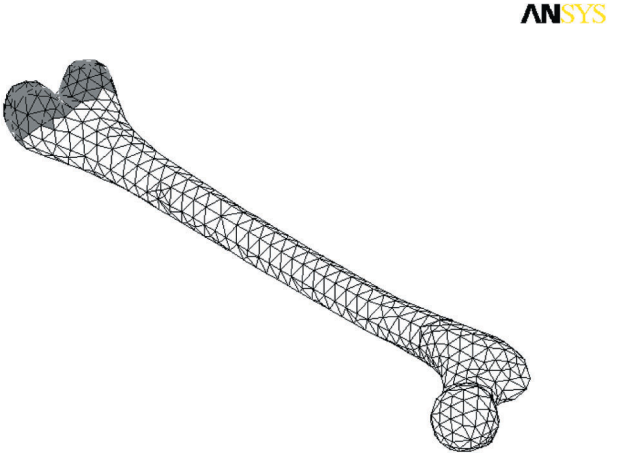

Figure 4. The boundary condition, applied to the model of the femur, was full constraint of all degrees of freedom at the nodes (dark gray) that lie at the distal end of the femur (knee joint).

Force (kN)	Point	X	Y	Z
Hip contact	P0	-0.383	-0.167	-1.286
Abductor	P1	0.693	0.035	0.723
Tensor fascia latae, prox.	P1	0.06	0.097	0.110
Tensor fascia latae, distal	P1	0.0042	-0.006	-0.159
Vastus lateralis	P2	-0.0076	0.155	-0.781

Table 1. Values and application points of joint reaction and muscle forces of the loading profile, which corresponds to the single instant of maximum *in vivo* hip contact force in the walking cycle.

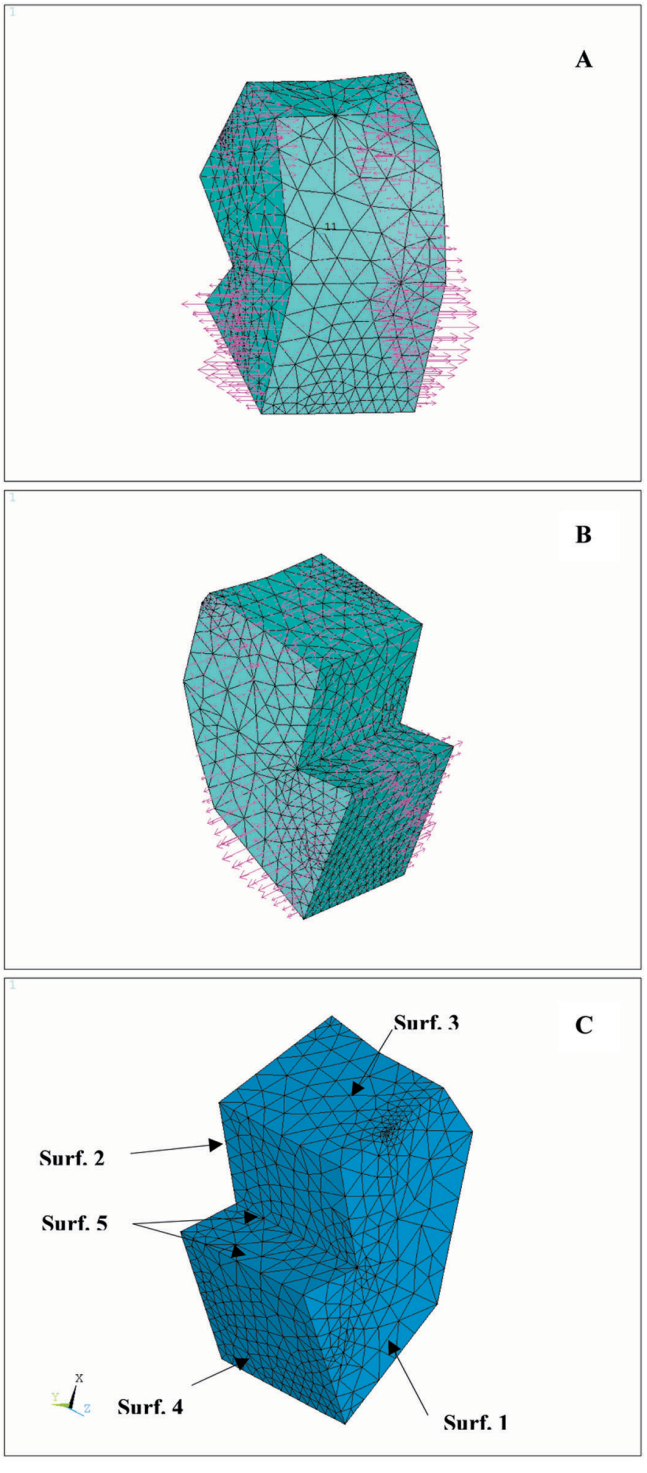

Figure 5. Mesoscale analysis. **A, B.** The finite element model and the forces which were used as external loads on each particular mesoscopic node. These forces were developed as a result of the analysis of the macroscopic model at a certain point of analysis (white cube, Figure 1). **C.** The surfaces of the mesoscale model on which the resultants of forces and moments of the Table 2 are applied.

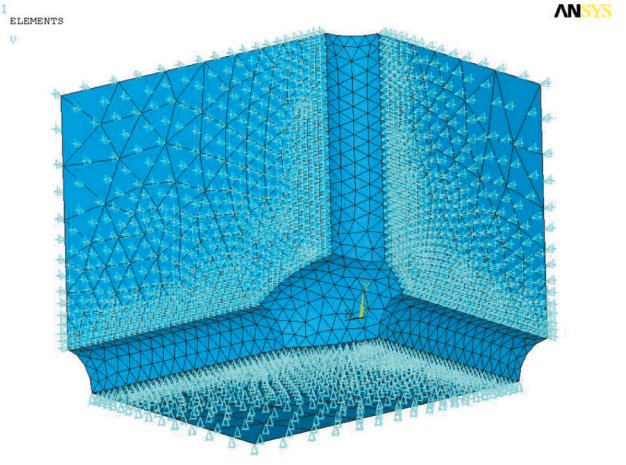

Figure 6. Microscopic model of the bone. The discritization with finite elements and the applied boundary conditions. Axial symmetry was utilized and only one-eighth of the model of Figure 2 was used by virtue of symmetry.

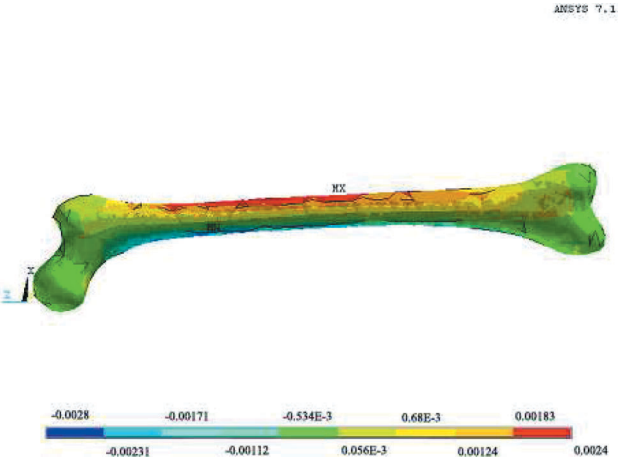

Figure 7. Prediction of the longitudinal macroscopic strain of a left femur (anterior view), following application of a loading configuration, corresponding to one-legged stance. Red areas indicate higher tensile strain whereas blue areas indicate higher compressive strain.

groups of canaliculi. The long axis of the ellipsoid lacuna in the microscopic model was directed to the circumferential direction of the cross-section of the femur. The microstructure representative volume with the details of its geometry is displayed in Figure 2. The dimensions of the lacunar axes are also included in Figure 2. The geometry of the model has been highly idealized. Confocal microscopy images of the lacunae suggest that an ellipsoidal model of the lacuna is a reasonable estimate[18]. McCreadie et al. (2004) have measured lacunar major axis from about 7 to 14 μm in not fractured female indi-

	Surface				
Force	**1**	**2**	**3**	**4**	**5**
F_x (kN)	-0.549	0.589	0.031	-0.073	-0.002
F_y (kN)	-0.039	0.039	-0.007	0.011	-0.010
F_z (kN)	1.813	-1.947	-0.329	0.576	-0.024
M_x (kN.cm)	98.218	-106.121	-22.197	37.824	-3.792
M_y (kN.cm)	5.542	-10.116	19.484	-22.772	2.217
M_z (kN.cm)	28.316	-30.668	-2.584	5.282	-0.622

Table 2. The resultants of forces and moments and the surfaces of the mesoscale model on which they are applied are presented (Figure 5). These forces are calculated from the local macroscopic stress assigned to a certain macroscopic point of analysis (Figure 1) and were used as external loads at the mesoscale analysis.

Stress component	Principal stress (MPa)
X	-0.43
Y	-0.52
Z	-35.89

Table 3. The assessed from the mesoscopic scale analysis local stress, assigned to a certain point (Figure 1), which was used to calculate the microscopic nodal forces, is presented.

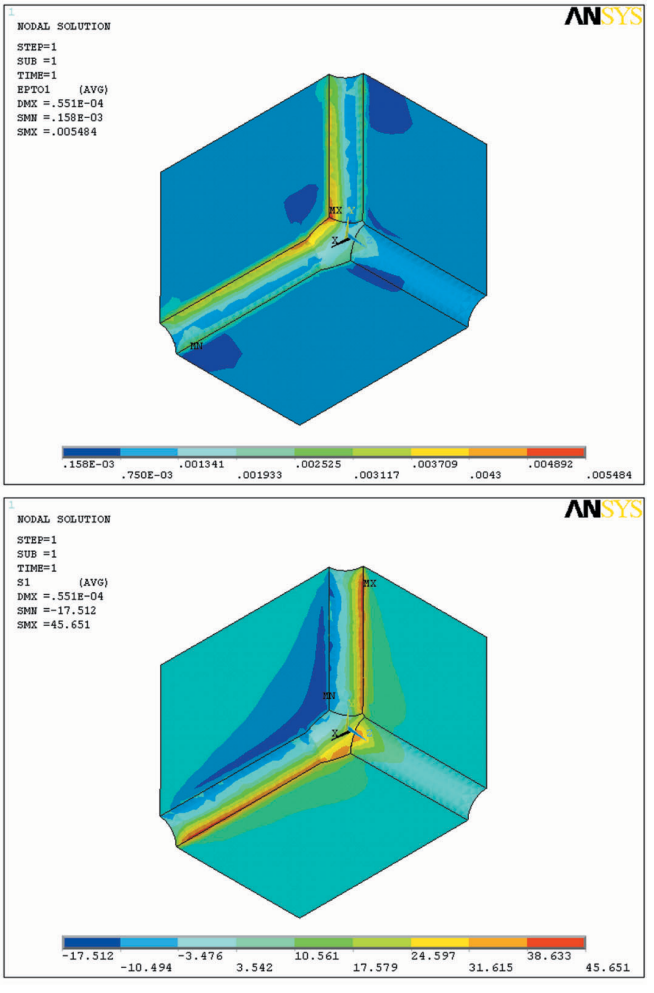

Figure 8. Prediction of the principal strain and stress I in the environment of an osteocyte within the extracellular matrix, following application of a loading configuration, corresponding to one-legged stance, at the diaphysis of the femur, where the maximum macroscopic compressive longitudinal strain was observed, for geometry 2. The values of stresses are in MPa.

viduals. In our measurements from a male iliac crest, lacunar long axis was found as long as 15 μm, and anisotropy was almost constant throughout the examined region. Based on this result, the anisotropy ratio was kept constant and the size of the long axis of the lacuna varied from 10 to 20 μm.

The dimensions of the other microstructural elements (canaliculi, canals, etc.) were obtained from measurements in two-dimensional images of stained transverse sections of a human femur diaphysis. The radius of the Haversian canal was taken to be 25 μm, the distance between two adjacent Haversian canals 200 μm and the width of the canalicular channel was taken to be 5 μm. This latter canalicular channel represents a group of 10 canaliculi, taken together as a single canaliculus. It was assumed that cells do not contribute to the mechanical properties of the tissue. For the discritization of the microscale models, the same element type (SOLID 92) was used as for the macroscale model. An axisymmetric model was utilized and only one-eighth of the microstructure representative volume was used by virtue of symmetry (Figure 6). A total of 11,561 elements were created. The assessed from the mesoscopic scale analysis local stress, assigned to a certain point, was used to calculate the microscopic nodal forces. A linear interpolation of the values of stress was applied to the nodal points on the faces of the microscale model. These stress values are presented in Table 3 and the nodal forces, used as suitable boundary conditions for the solution of the symmetric problem, are depicted in Figure 6. This technique assumes that the changes in stress and strain fields within the microscale mesh caused by the presence of the lacuna and the canaliculi are not apparent at the edges of the mesh. The microstructure can be thought of as repeating itself near a mesoscopic point. However, the microstructure may differ from one mesoscopic point to another.

The solid bone material at the microscopic level was also assumed to be transversely isotropic. For the determination of the values of elastic moduli at this level, an iteration procedure was followed: The strain field was determined from the solution of the microscopic FE model and the imposed at the nodes forces calculated from the transferred mesoscopic stresses. If the calculated displacements at the microscopic nodes do not coincide with those calculated from the mesoscopic analysis, the modulus of elasticity is gradually increased

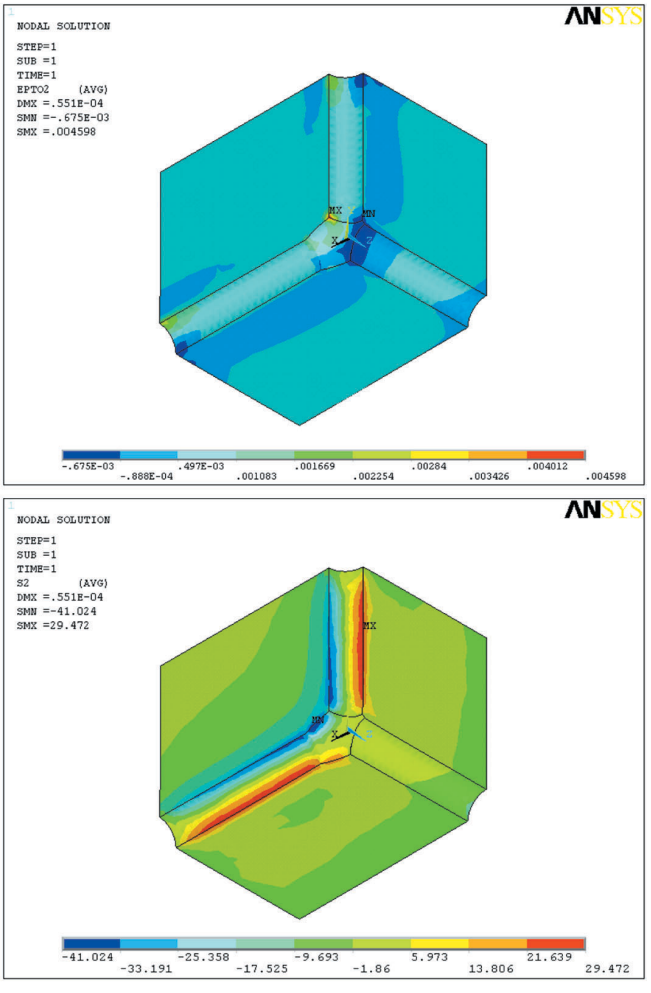

Figure 9. Prediction of the principal strain and stress II in the environment of an osteocyte within the extracellular matrix, following application of a loading configuration, corresponding to one-legged stance, at the diaphysis of the femur, where the maximum macroscopic compressive longitudinal strain was observed, for geometry 2. The values of stresses are in MPa.

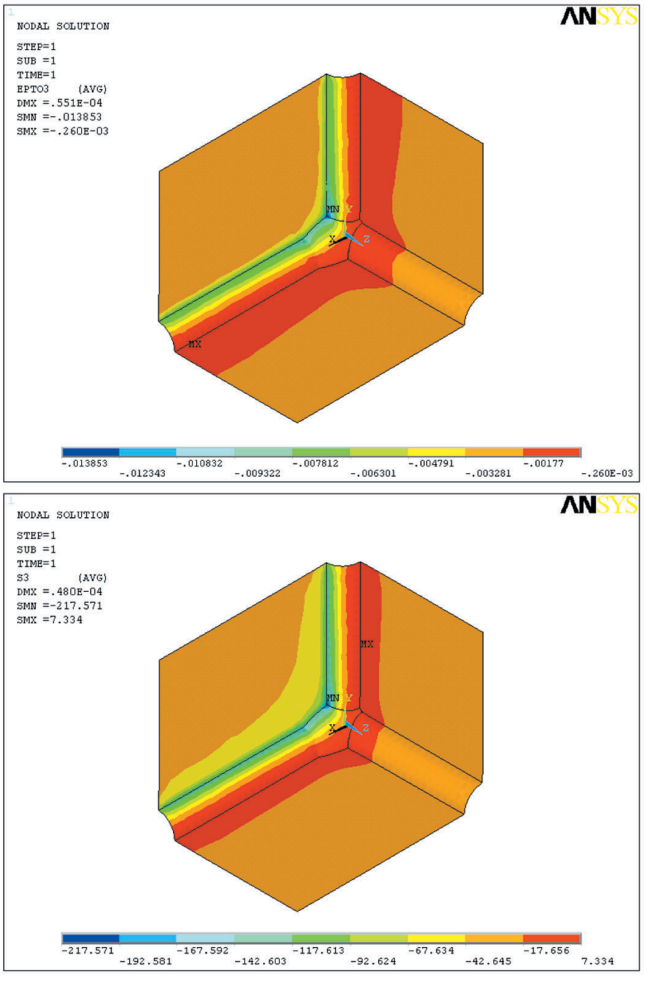

Figure 10. Prediction of the principal strain and stress III in the environment of an osteocyte within the extracellular matrix, following application of a loading configuration, corresponding to one-legged stance, at the diaphysis of the femur, where the maximum macroscopic compressive longitudinal strain was observed, for geometry 2. The values of stresses are in MPa.

and the procedure is continued to arrive at an updated estimation of the microscopic displacement field, until convergence is succeeded. The calculated in this way elastic modulus was found 10% increased relatively to the macroscopic one. This can be attributed to lack of microporosity at this level.

The computational engine itself at the microscale was validated by computing the stress and strain field for the simplified case of an included spherical hole subjected to a uniform stress and comparing this result with the analytical solution.

Results

The used loading configuration, representing one legged-stance and taking into consideration the abductors, the tensor fascia latae and the vastus lateralis muscle groups, produced almost uniform strain distribution along the diaphysis and the longitudinal strain ranged between 2,400 (laterally) and -2,800 μstrain (medially) (Figure 7). The maximum tensile longitudinal strain was observed at the lateral diaphysis and the maximum compressive longitudinal strain at the medial diaphysis and did not exceed 2,800 μstrain. The actual tissue principal strain along the femur deviated considerably from an average tissue value.

Figures 8-10 display the prediction of the principal local tissue stresses and strains on a cellular level at the diaphysis of the femur, where the maximum macroscopic compressive longitudinal strain was observed, for major and minor axes 15 μm and 7.5 μm, respectively (geometry 2). For all three geometries the predicted stresses and strains in the area of the lacunae, were nonuniform and differed significantly from those in the bulk extracellular matrix. The local strain in the area surrounding

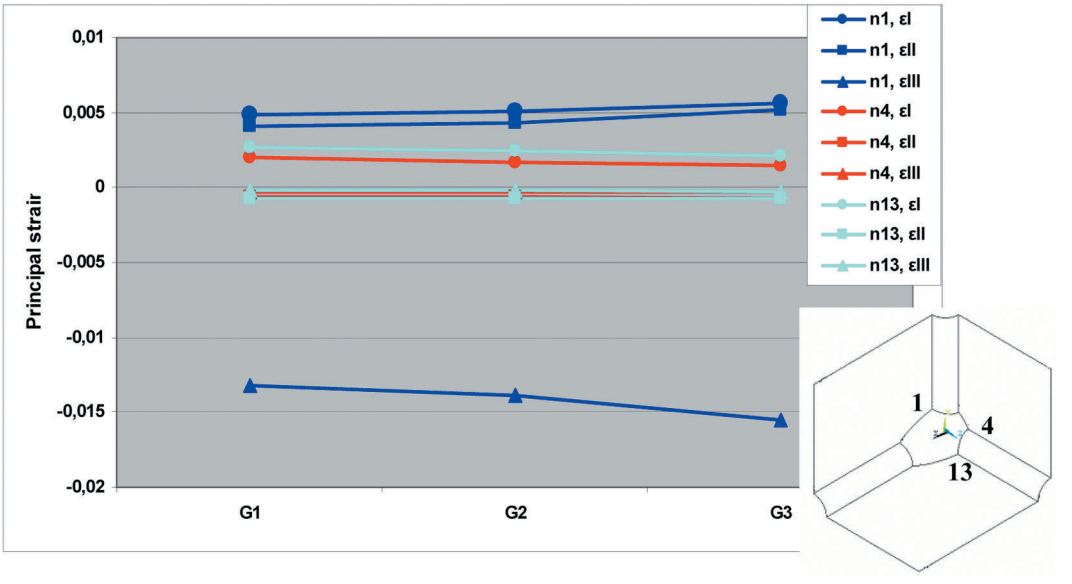

Figure 11. Influence of lacunar axes dimensions (G1, G2 and G3) on local tissue principal strain (I, II and III) at the periphery of the lacuna at nodes 1, 4 and 13.

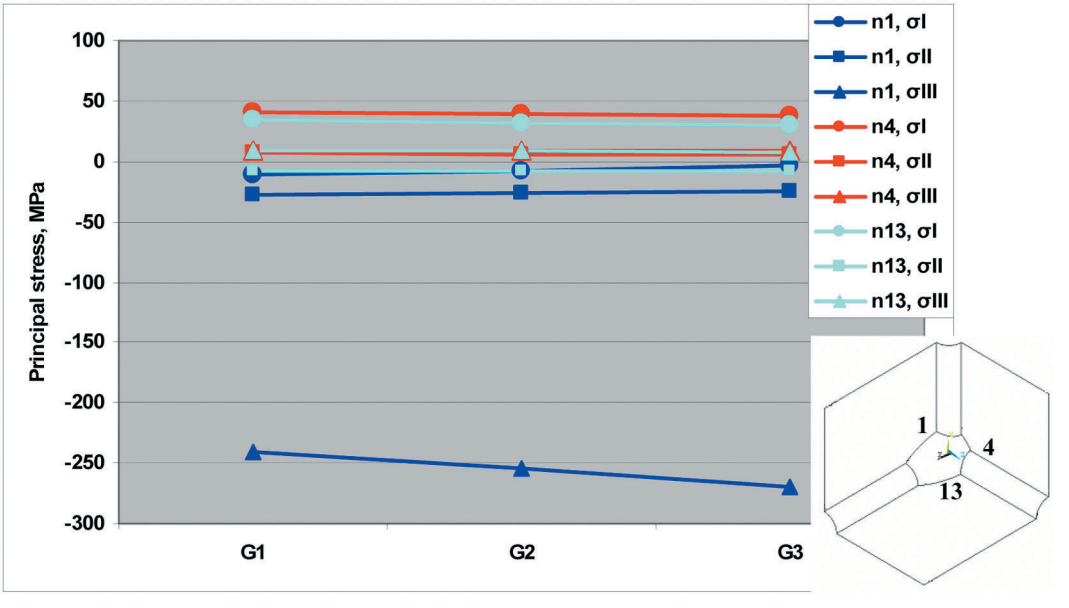

Figure 12. Influence of lacunar axes dimensions (G1, G2 and G3) on local tissue principal stresses (I, II and III) at the periphery of the lacuna at nodes 1, 4 and 13.

the lacunae was considerably larger in comparison to literature values obtained from *in vivo* strain-gauge measurements in human bone (Lanyon et al., 1975). Peak stresses and strains in the walls of the lacuna were up to six times those in the bulk extracellular matrix. The maximum compressive strain, of the order of 10,000 μstrain, was observed along canaliculi and particularly at sites where the process meets the cell body.

Figures 11 and 12 display the influence of lacunar major and minor axes dimensions on local tissue stress and strain at the nodes 1, 4 and 13. The lacunar size increased or decreased the tissue strain, depending on the location and the direction. The maximum compressive strain was observed at node 1 and its value increased at 3.5% with an increase of the major lacunar axis from 10 μm to 20 μm.

		G1	G2	G3
Node 1	σ_I	-11,0	-7,5	-4,0
	σ_{II}	-28,0	-26,0	-25,0
	σ_{III}	-240,0	-25,0	-270,0
Node 4	σ_I	40,0	38,6	37,0
	σ_{II}	6,5	5,9	5,7
	σ_{III}	8,0	8,3	8,9
Node 13	σ_I	34,0	31,6	30,0
	σ_{II}	-8,3	-8,0	-8,2
	σ_{III}	8,4	8,1	7,4

Table 4. Local tissue principal stress (I, II and III) at the periphery of the lacuna at nodes 1, 4 and 13, for each set of lacunar axes dimensions (G1, G2 and G3).

		G1	G2	G3
Node 1	ε_I	4850	5100	5650
	ε_{II}	4100	4300	5150
	ε_{III}	-13200	-13900	-15500
Node 4	ε_I	2031	1733	1431
	ε_{II}	-620	-680	-740
	ε_{III}	-300	-270	-250
Node 13	ε_I	2658	2400	2085
	ε_{II}	-720	-730	-740
	ε_{III}	-170	-210	-250

Table 5. Local tissue principal strain (I, II and III) at the periphery of the lacuna at nodes 1, 4 and 13, for each set of lacunar axes dimensions (G1, G2 and G3).

Discussion

Cells are constantly subjected to mechanical stimuli. Though many studies have been performed *in vitro* to investigate the mechanisms of detection and adaptation to mechanical strains, the cellular strains remain largely unknown. Most researchers regard as physiological osteocyte deformation the measured bone surface strains[20-22]. However, the stress-strain fields in the vicinity of the cell cannot be established *a priori* from macroscopic tissue strains, as cells experience a complex stress and strain state caused by the heterogeneous microstructural architecture and the physical behaviour of both cells and extracellular matrix. Since cellular deformation is likely involved in mechanical adaptation and remodeling, further understanding of the biomechanical origins of alterations in cellular responses can be aided by the use of computational models.

In this work, a multilevel biomechanical finite element model has been developed to determine the strain in the area of an individual cell and the canalicular processes during the stance phase of gait cycle. The multilevel approach has been validated and proven to be successful for describing technical materials. The effective macroscopic tissue behavior is derived from the microstructural calculations by a computational homogenization procedure[10,12]. Using this homogenization procedure, the effective material properties can be computed for arbitrary complex microstructural material behavior and cell geometries, even under large strain conditions. In our model, an opposite procedure is followed: the local cell deformations are determined by detailed linear finite element analysis of the heterogeneous microstructure, from the external loading of the macrostructure. A similar procedure was followed by Guilak et al. (2000) in a macro-micro finite element model for describing the local mechanical environment of chondrocytes in articular cartilage.

This model incorporates a detailed analysis of the complex microstructure of cortical bone, consisting of an arrangement of cells embedded in matrix material. This has the advantage that influences of porosity, cell distribution and cell geometry on local strain can be studied. The geometry of the model has been highly idealized. Lacunar ellipsoid shape and perpendicular emanating of canaliculi from a lacuna are reasonable representations of bone microstructure as it has been illustrated by confocal microscopy images and microphotographs under reflected polarized light[18,23]. Local periodicity has been assumed in most micromechanical models of bone microstructure[24,25]. An advantage of this model is that it is 3-dimensional in order to take into account the known local anisotropy behaviour of the bone tissue.

Overall good agreement was observed between the present numerical results for the whole femur and those of previous solutions. The strain magnitudes determined from this finite element analysis appear comparable to those determined from *in vivo* measurements by strain gauges on tibial shaft surface[19,26,27] (up to 2,500 μstrain in humans), by *in vitro* measurements on embalmed or synthetic femur models[28] or by FE modeling[28,29]. The maximum principal strain of the current study was about 7% higher than that found by Speirs et al. (2007), when physiological boundary conditions were applied. The difference can be attributed to the anisotropic elastic modulus adopted in the current study.

The strain at the osteocytes level during a usual daily loading may be up to six times higher than the nominal values predicted for the extracellular matrix and this strain does not depend strongly on lacunar size. An increase of the long lacunar axis from 10 μm to 20 μm increased the maximum compressive strain at 3.50%. The canalicular size does not influence strongly perilacunar strain. An increase of 2.31% in the predicted maximum strain has been observed with an increase in canalicular diameter from 0.362 to 0.421 μm[30]. The microscopic model was indirectly validated by comparison of its results to literature measurements. The strain values, calculated by the FE model at the microscopic level, were comparable to those found by direct *in situ* measurements of the deformation behavior of cortical bone specimens. A nominal continuum strain level on bone specimens

approximately equal to that measured in humans *in vivo*, was found that produced local, osteocyte level, strains as high as 12,000 to 15,000 μstrain[4].

A point of criticism might concern the maximum strain that bone can withstand without failure. Tensile microcracks were found that first appear at approximately 4,000 μstrain, and considerable growth in microcrack density appeared once the tensile strain has passed 8,000 μstrain. Compressive microcracks were first formed at higher macroscopic strains 8,000-10,000 μstrain[31]. These are macroscopic strains calculated from load-deformation curves of the specimens, and they are average over the measured area. Local regions in bone, like lacunae, erosion areas, microcracks, can develop much higher local strain. According to these findings, even the estimated by our model maximum strain of 10,000 μstrain may not be catastrophic to bone. Microcracks have been observed to initiate frequently at osteocyte lacunae[32] providing evidence that strain in the matrix around osteocytes is considerably higher than in the rest of the tissue. The findings of the current work are consistent with the above experimental results.

Cell responses are found to depend on the magnitude and form of the applied strains. In most studies the levels of strain magnitude applied *in vitro* to cells to elicit responses are those measured experimentally by strain gauges *in vivo* on the external bone surfaces (2,500 μstrain) and these strains are considered as physiological. According to the results of this study as well of other studies[4,8,24] much higher strains, considered as supraphysiological, can be developed in bone at the osteocyte level during a usual activity like gait. Thus, the very high deformation found *in vitro* necessary to activate a direct mechanotransduction might indeed be observed in physiological conditions at the cell level, because of the local strain amplification.

The current model can be refined in the future by including additional microstructural characteristics (various sizes of lacunae and a larger number of canaliculi with smaller diameters) and extended to include influence of pericellular non-mineralized matrix, fluid flow, or even the influence of the cell properties on the stress-strain fields within the extracellular matrix.

References

1. Cowin SC, Moss-Salentijn L, Moss ML. Candidates for the mechanosensory system in bone. J Biomech Eng 1991;115:191-7.
2. Owan I, Burr DB, Turner CH, Qiu J, Tu Y, Onyia JE, Duncan RL. Mechanotransduction in bone: osteoblasts are more responsive to fluid forces than mechanical strain. Am J Physiol 1997;273:C810-5.
3. You J, Yellowley CE, Donahue HJ, Zhang Y, Chen Q, Jacobs CR. Substrate deformation levels associated with routine physical activity are less stimulatory to bone cells relative to loading-induced oscillatory fluid flow. J Biomech Eng 2000;122:387-93.
4. Nicolella DP, Lankford J. Microstructural strain near osteocyte lacuna in cortical bone *in vitro*. J Musculoskelet Neuronal Interact 2002;2:261-3.
5. Nicolella DP, Moravits DE, Gale AM, Bonewald LF, Lankford J. Osteocyte lacunae tissue strain in cortical bone. J Biomech 2006;39:1735-43.
6. Van Rietbergen B, Müller R, Ulrich D, Rüegsegger P, Huiskes R. Tissue stresses and strain in trabeculae of a canine proximal femur can be quantified from computer reconstructions [corrected and republished in J Biomech 1999;32:443-51]. J Biomech 1999;32:165-73.
7. Hollister SJ, Brennan JM, Kikuchi N. A homogenization sampling procedure for calculating trabecular bone effective stiffness and tissue level stress. J Biomech 1994;27:433-44.
8. Deligianni DD, Apostolopoulos CA. Multilevel finite element modeling for the prediction of local cellular deformation in bone. Biomech Model Mechanobiol 2008;7:151-9.
9. Duda GN, Heller M, Albinger J, Schulz O, Schneider E, Claes L. Influence of muscle forces on femoral strain distribution. J Biomech 1998;31:841-6.
10. Kouznetsova V, Brekelmans WAM, Baaijens FPT. An approach to micro-macro modeling of heterogeneous materials. Computational Mechanics 2001;27:37-48.
11. Guilak F and Mow VC. The mechanical environment of the chondrocyte: a biphasic finite element model of cell-matrix interactions in articular cartilage. J Biomech 2000;33:1663-73.
12. Breuls RGM, Sengers BG, Oomens CWJ, Bouten CVC, Baaijens FPT. Predicting local cell deformations in engineered tissue constructs: a multilevel finite element approach. Trans ASME 2002;124:198-207.
13. Ashman RB, Cowin SC, Van Buskirk WC, Rice JC. A continuous wave technique for the measurement of the elastic properties of cortical bone. J Biomech 1984; 17:349-61.
14. Wirtz DC, Schiffers N, Pandorf T, Radermacher K, Weichert D, Forst R. Critical evaluation of known bone material properties to realize anisotropic FE-simulation of the proximal femur. J Biomech 2000;33:1325-30.
15. Cheung G, Zalzal P, Bhandari M, Spelt JK, Papini M. Finite element analysis of a femoral retrograde intramedullary nail subject to gait loading. Med Eng Phys 2004;26:93-108.
16. Taylor WR, Roland E, Ploeg H, Hertig D, Klabunde R, Warner MD, Hobatho MC, Rakotomanana L, Clift SE. Determination of orthotropic bone elastic constants using FEA and modal analysis. J Biomech 2002;35:767-73.
17. Heller MO, Bergmann G, Kassi J-P, Claes L, Haas NP, Duda GN. Determination of muscle loading at the hip joint for use in pre-clinical testing. J Biomech 2005; 38:1155-63.
18. McCreadie BR, Hollister SJ, Schaffler MB, Goldstein SA. Osteocyte lacuna size and shape in women with and without osteoporotic fracture. J Biomech 2004;37:563-72.

19. Lanyon LE, Hampson WE Jr, Goodship AE, Shah JS. Bone deformation recorded *in vivo* from strain gauges attached to the human tibial shaft. Acta Orthop Scand 1975;46:256-68.
20. Kaspar D, Seidl W, Neidlinger-Wilke C, Claes L. *In vitro* effects of dynamic strain on the proliferative and metabolic activity of human osteoblasts. J Musculoskelet Neuronal Interact 2000;1:161-4.
21. Tang LL, Wang YL, Pan J, Cai SX. The effect of stepwise increased stretching on rat calvarial osteoblast collagen production. J Biomech 2004;37:157-61.
22. Di Palma F, Guignandon A, Chamson A, Lafage-Proust MH, Laroche N, Peyroche S, Vico L, Rattner A. Modulation of the responses of human osteoblast-like cells to physiologic mechanical strains by biomaterials surfaces. Biomaterials 2005;26:4249-57.
23. Marotti G, Remaggi F, Zaffe D. Quantitative investigation on osteocyte canaliculi in human compact and spongy bone. Bone 1985;6:335-7.
24. Bonivtch AR, Bonewald LF, Nicolella DP. Tissue strain amplification at the osteocyte lacuna: a microstructural finite element analysis. J Biomech 2007;40:2199-206.
25. Mak AFT, Huang DT, Zhang JD, Tong P. Deformation-induced hierarchical flows and drag forces in bone canaliculi and matrix microporosity. J Biomech 1997;30:11-8.
26. Brand RA, Stanford CM, Nicolella DP. Primary adult human bone cells do not respond to tissue (continuum) level strains. J Orthop Sci 2001;6:295-301.
27. Burr DB, Milgrom C, Fyhrie D, Forwood M, Nyska M, Finestone A, Hoshaw S, Saiag E, Simkin A. *In vivo* measurement of human tibial strains during vigorous activity. Bone 1996;18:405-10.
28. Cristofolini L, Cappollo A, McNamara BP, Viceconti M. A minimal parametric model of the femur to describe axial elastic strain in response to loads. Med Eng Phys 1996;18: 502-14.
29. Speirs AD, Heller MO, Duda GN, Taylor WR. Physiologically based boundary conditions in finite element modeling. J Biomech 2007;40:2318-23.
30. Bonivtch AR, Bonewald LF, Nicolella DP. Tissue strain amplification at the osteocyte lacuna: A microstructural finite element analysis. J Biomech 2007;40:2199-206.
31. Reilly GC, Currey JD. The development of microcracking and failure in bone depends on the loading mode to which it is adapted. J Exper Biol 1999;202:543-52.
32. Reilly GC. Observations of microdamage around osteocyte launae in bone. J Biomech 2000;33:1131-4.